ration. In this case, variations in the ratio of photo/dark respiration may cause some changes in Δ_{max}, especially in conditions of inorganic carbon limitation favorable to photorespiration such as in terrestrial C_3 vegetation. However, aquatic plants developed mechanisms to concentrate CO_2 and suppress photorespiration [A. Kaplan and L. Reinhold, *Annu. Rev. Plant Physiol. Plant Mol. Biol.* **50**, 539 (1999)]. As a result, photorespiration is not likely to affect oceanic Δ_{max}.

11. H. Craig and L. I. Gordon, in *Conference on Stable Isotopes in Oceanographic Studies and Paleotemperatures*, E. Tongiorgi, Ed. (Laboratory of Geology and Nuclear Science, Pisa, Italy, 1965), pp. 9–130.
12. Air-water equilibrium was attained in less than 24 hours by bubbling outside air into seawater (25°C). The Δ_{eq} value was determined in five separate experiments. Its average value was 16 per meg with a standard error of ±2 per meg. For simplicity in calculations we assumed that the deviation of Δ_{eq} from zero is the result of isotopic fractionation occurring only during O_2 invasion. In the cases discussed here, errors due to this assumption are negligible.
13. J. F. Clark *et al.*, in *Air-Water Gas Transfer*, B. Jaehne and E. C. Monahan, Eds. (Aeon Verlag & Studio, Hanau, Germany, 1995), pp. 785–800.
14. P. D. Nightingale *et al.*, *Global Biogeochem. Cycles* **14**, 373 (2000).
15. H. Craig and T. Hayward, *Science* **235**, 199 (1987).
16. W. J. Jenkins and J. C. Goldman, *J. Mar. Res.* **43**, 465 (1985); W. S. Spitzer and W. S. Jenkins, *J. Mar. Res.* **47**, 169 (1989).
17. B. Luz and E. Barkan, data not shown.
18. A. F. Michaels and A. H. Knap, *Deep-Sea Res. II* **43**, 157 (1996); S. C. Doney, D. M. Glover, R. G. Najjar, *Deep-Sea Res. II* **43**, 591 (1996).
19. B. B. Benson and D. Krause Jr., *Limnol. Oceanogr.* **29**, 620 (1984).
20. Data is found at www.bbsr.edu/Weather/climatology.html; R. Wanninkhof, *J. Geophys. Res.* **97**, 7373 (1992).
21. We are grateful to M. Bender for numerous discussions on all aspects of this research. Comments by A. Kaplan, Y. Kolodny, and three anonymous reviewers significantly improved the manuscript. We appreciate the help of the Bermuda Biological Station in sampling at BATS and extend special thanks to S. Bell. The support of the Kinneret National Laboratory is appreciated. Y. Yacobi and Y. Sagi helped in gross-production measurements in the Sea of Galilee, and J. Erez and K. Schneider helped with the coral experiment. The support of the U.S.-Israel Binational Science Foundation, The Israel Science Foundation, MARS-2, and the Moshe-Shilo Minerva Center is greatly appreciated.

6 December 1999; accepted 11 May 2000

A Low-Operating-Temperature Solid Oxide Fuel Cell in Hydrocarbon-Air Mixtures

Takashi Hibino,[1]* Atsuko Hashimoto,[1] Takao Inoue,[2] Jun-ichi Tokuno,[2] Shin-ichiro Yoshida,[2] Mitsuru Sano[2]

The performance of a single-chamber solid oxide fuel cell was studied using a ceria-based solid electrolyte at temperatures below 773 kelvin. Electromotive forces of ~900 millivolts were generated from the cell in a flowing mixture of ethane or propane and air, where the solid electrolyte functioned as a purely ionic conductor. The electrode-reaction resistance was negligibly small in the total internal resistances of the cell. The resulting peak power density reached 403 and 101 milliwatts per square centimeter at 773 and 623 kelvin, respectively.

Fuel cells are widely viewed as a promising source of low-emission power generation for vehicles. There is great controversy over which fuel should be used. Polymer electrolyte fuel cells (PEFCs) exhibit high power densities at low temperatures (~353 K), but they require hydrogen as the fuel, which is impractical in terms of storage and handling. An external reformer can be used to convert alcohols and hydrocarbons into hydrogen, but their portability is inferior. There have been recent successes with solid oxide fuel cells (SOFCs), which perform well between 823 and 973 K using methane (*1*) and *n*-butane (*2*) directly as the fuels. A further reduction in the operating temperature of SOFCs and an enhancement in their thermal and mechanical shock resistance would make this technology a promising alternative to PEFCs.

A type of fuel cell that consists of only one gas chamber, where both the anode and the cathode are exposed to the same mixture of fuel and air, has been proposed by many researchers (*3–8*). This design is more shock resistant than conventional fuel cells, both thermally and mechanically. We have recently succeeded in applying this single-chamber cell design to a SOFC constructed from yttria-stabilized zirconia (YSZ), which is commonly used as a solid electrolyte in SOFCs, with a Ni-based anode and a perovskite cathode (*9*). This SOFC, however, must operate at the high temperature of 1223 K to achieve sufficient ionic conduction in the solid electrolyte.

Different cation-doped ceria, notably samaria-doped ceria (SDC), have much higher ionic conduction than YSZ in an oxidizing atmosphere, whereas they show n-type semiconduction in a reducing atmosphere (*10, 11*). Because the resulting electromotive force (EMF) of the SOFC is lower than the theoretical value, the SDC electrolyte has so far been regarded as unsuitable for such applications. However, the partial pressure of oxygen at the boundary of the two atmospheres becomes gradually lower as the operating temperature decreases (*12*), which suggests that the SDC electrolyte can be used even under fuel cell conditions, provided it operates at extremely low temperatures. In this report, we demonstrate a low-temperature SOFC by combining the advantages of the SDC electrolyte with the single-chamber cell design.

The SDC electrolyte we used here was prepared by pressing a commercial ceramic powder, $Ce_{0.8}Sm_{0.2}O_{1.9}$ (Anan Kasei Co. Ltd.), hydrostatically into a pellet at 2×10^3 kg cm^{-2} and then sintering in air at 1773 K for 10 hours. After the pellet was cut into a disk (diameter 14 mm, thickness ~1 mm), the SDC disk surface was polished to a given thickness (0.15 to 0.50 mm) with an abrasive paper. YSZ (8 mol% yttria) and $La_{0.9}Sr_{0.1}Gd_{0.8}Mg_{0.2}O_3$ (LSGM) were used as solid electrolytes for comparison. Preliminary experiments revealed that 10 weight % SDC–containing Ni and $Sm_{0.5}Sr_{0.5}CoO_3$ electrodes best functioned as the anode and the cathode, respectively. These pastes were smeared on the opposite surfaces (area 0.5 cm^2) of the SDC disk, followed by calcining in air at 1223 K for 4 hours. The cell thus fabricated was placed in an alumina tube (inner and outer diameters 15 and 19 mm, respectively). Methane, ethane, and propane were mixed with air for each of the respective concentrations—30 volume % for methane, 18 volume % for ethane, and 14 volume % for propane—so that the oxidation would proceed safely without exploding (the explosive limits of methane, ethane, and propane in air are 15.0, 12.5, and 9.5 volume %, respectively). The gas mixture was supplied to the cell at flow rates of 300 ml min^{-1} between 623 and 773 K (Fig. 1).

When the single-chamber SOFCs using SDC, YSZ, and LSGM with a thickness of 0.50 mm were supplied with a mixture of ethane and air at 773 K, all three cells generated stable EMFs of ~920 mV, where the

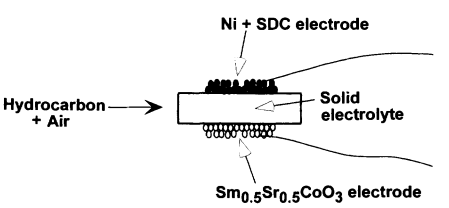

Fig. 1. A schematic illustration of single-chamber SOFC in a flowing mixture of hydrocarbon and air.

[1]Department of Structure Formation Process, National Industrial Research Institute of Nagoya, Nagoya 462-8510, Japan. [2]Graduate School of Human Information, Nagoya University, Nagoya 466-0804, Japan.

*To whom correspondence should be addressed. E-mail: thibino@nirin.go.jp

potential of the 10 weight % SDC–containing Ni electrode was negative versus the $Sm_{0.5}Sr_{0.5}CoO_3$ electrode (Fig. 2). From the analysis of the outlet gas from the cell having only the 10 weight % SDC–containing Ni or $Sm_{0.5}Sr_{0.5}CoO_3$ electrode, it was found that the partial oxidation of ethane by oxygen proceeded to form a large amount of hydrogen and carbon monoxide over the 10 weight % SDC–containing Ni electrodes, whereas such an oxidation proceeded at a very slow rate over the $Sm_{0.5}Sr_{0.5}CoO_3$ electrode. Therefore, it can be predicted that the potential of the 10 weight % SDC–containing Ni electrode is determined by the partial pressure of oxygen in its vicinity after the following reactions attain equilibrium:

$$C_2H_6 + O_2 \rightarrow 3H_2 + 2CO \quad (1)$$

$$H_2 + O^{2-} \rightarrow H_2O + 2e^- \quad (2)$$

$$CO + O^{2-} \rightarrow CO_2 + 2e^- \quad (3)$$

[For details on Eq. 1, see (*13*).] Hence, this electrode will show a significantly negative potential. On the other hand, the potential of the $Sm_{0.5}Sr_{0.5}CoO_3$ electrode is a mixed potential based on the following reactions:

$$\tfrac{1}{2}O_2 + 2e^- \rightarrow O^{2-} \quad (4)$$

$$C_2H_6 + 2O^{2-} \rightarrow 3H_2 + 2CO + 4e^- \quad (5)$$

or

$$C_2H_6 + 7O^{2-} \rightarrow 3H_2O + 2CO_2 + 14e^- \quad (6)$$

The large EMF values stated above, however, suggest that this electrode favors Eq. 4 rather than Eqs. 5 or 6, because the potential determined by Eq. 4 is much less negative than those determined by Eqs. 5 and 6.

The similarity in EMF values among the three cells (Fig. 2) means that the SDC behaved as a purely ionic conductor during operation in a similar manner to the other solid electrolytes [the equilibrium partial pressure of oxygen in the gas mixture under the present conditions, $\sim 10^{-19}$ atoms, is in the range of the electrolytic domain at 773 K (*12*)]. Although current could be drawn from the three cells, the voltage drop was the least in the cell using the SDC. The impedance spectra of the three cells further clarified this point (Fig. 3). The order of the ohmic resistance was SDC < LSGM < YSZ, which can be predicted from their ionic conductivities at 773 K. More important was the extremely small electrode-reaction resistance of 0.24 ohms observed on the cell using the SDC, suggesting that the cell performance would be improved using an even thinner SDC film. It has been reported that when the charge transfer reaction at the three-phase (gas-electrode-electrolyte) boundary is a rate-determining step in the electrode reaction, the anodic or cathodic reactions (or both) are promoted as the ionic conductivity of the solid electrolyte increases (*14*), which best explains why the cell using the SDC exhibited the smallest electrode-reaction resistance.

Evidence for the above suggestion is provided by the discharge properties of the single-chamber SOFC using SDC of different thicknesses in a flowing mixture of ethane and air at 773 K (Fig. 4). The voltage drop during cell discharge was strongly dependent on the thickness of the SDC, which resulted in an increasing power density with decreasing thickness of the SDC. In the cells using LSGM and YSZ, there was little correlation between the power density and the thickness of the solid electrolyte, because of their large electrode-reaction resistances. For example, the power density of the cell using LSGM increased

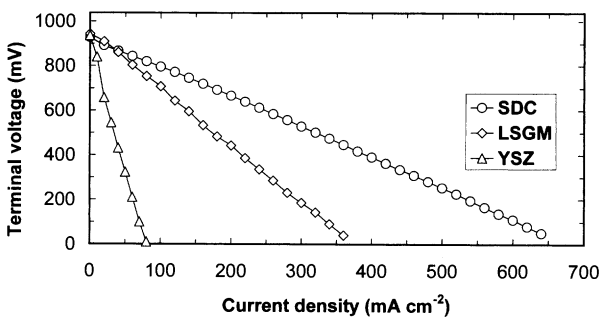

Fig. 2. Terminal voltage–current density curves of single-chamber SOFCs using SDC, YSZ, and LSGM with a thickness of 0.50 mm in a flowing mixture of ethane and air at 773 K. The gas mixture consisted of 52 ml min^{-1} ethane, 52 ml min^{-1} oxygen, and 196 ml min^{-1} nitrogen.

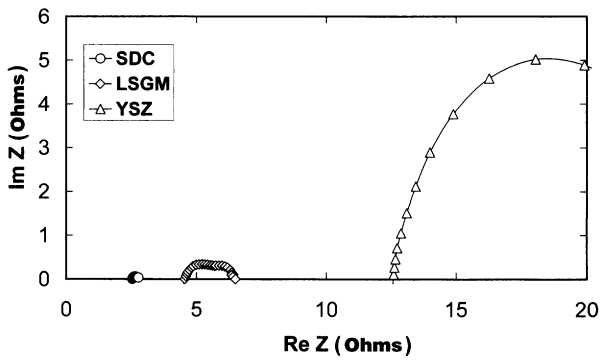

Fig. 3. Impedance spectra of single-chamber SOFCs using SDC, YSZ, and LSGM with a thickness of 0.50 mm in a flowing mixture of ethane and air at 773 K. These spectra were measured under open-circuit conditions by changing the frequency from 0.1 to 10^4 Hz. The impedance arcs correspond to the total electrode-reaction resistance in the cell.

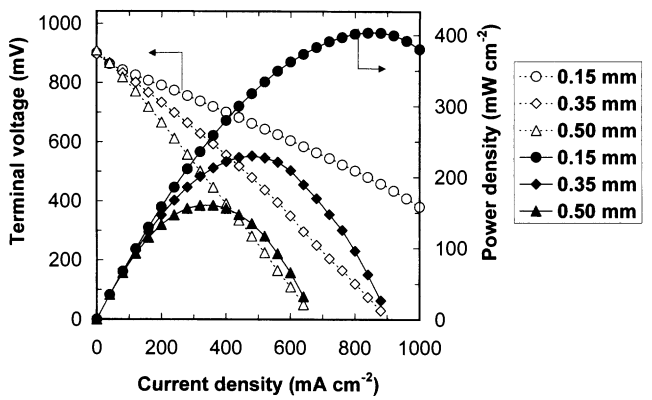

Fig. 4 (left). Discharge properties of single-chamber SOFCs using SDC of different thicknesses in a flowing mixture of ethane and air at 773 K. Experimental conditions are the same as in Fig. 2.

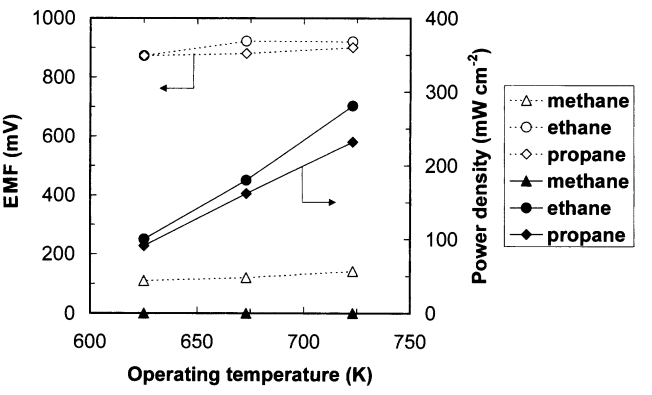

Fig. 5 (right). EMF and power density of single-chamber SOFCs using SDC with a thickness of 0.15 mm in a mixture of different hydrocarbons and air between 623 and 723 K. The mixture of methane and air consisted of 89 ml min^{-1} methane, 44 ml min^{-1} oxygen, and 167 ml min^{-1} nitrogen. The mixture of propane and air consisted of 41 ml min^{-1} propane, 54 ml min^{-1} oxygen, and 205 ml min^{-1} nitrogen.

from 90 to no more than 140 mW cm^{-2} as thickness decreased from 0.5 to 0.15 mm.

The partial oxidation of ethane represented by Eq. 1 is thermodynamically possible even below 773 K:

$$C_2H_6 + O_2 \rightarrow 3H_2 + 2CO$$

$$\Delta G°(673\ K) = -383\ kJ\ mol^{-1} \quad (7)$$

where $\Delta G°$ is Gibbs free energy. We therefore studied the performance of the single-chamber SOFC using SDC with a thickness of 0.15 mm under such conditions (Fig. 5). In the range of 623 to 723 K, the cell generated EMFs of ~900 mV, and the discharge properties were stable and reproducible. No carbon deposition was observed on the anode after operation. In addition, the impedance spectra of the cell showed small electrode-reaction resistances: 0.34 ohms for 723 K, 0.79 ohms for 673 K, and 1.64 ohms for 623 K. It appears that such fast electrode kinetics clean the precursors for carbon formation on the anode.

Figure 5 also shows the corresponding results for the other hydrocarbons. The cell performance in a mixture of propane and air was similar to that in a mixture of ethane and air, except at 723 K, where the $Sm_{0.5}Sr_{0.5}CoO_3$ electrode could not function well as the cathode, because this material was no longer inert to the oxidation of propane. On the other hand, the EMFs generated from the cell in a mixture of methane and air were only ~120 mV throughout the tested temperature range, where the oxidation rate of methane was too slow to form hydrogen and carbon monoxide over the 10 weight % SDC–containing Ni anode, probably causing a depression in Eqs. 2 and 3. We thus conclude that ethane and propane can be successfully used in the present SOFC at an operating temperature of 773 K or less. Because of their similar properties, we can assume that liquefied petroleum gas (LPG) or even butane would perform equally well.

The present SOFC has several additional advantages over PEFCs: (i) The anode is not subject to poisoning by carbon monoxide, whereas it is a critical problem for PEFCs (*15, 16*). (ii) There is no noble metal, such as Pt, in our SOFC, so fabrication costs are low. (iii) Although PEFCs themselves can operate at low temperatures, the hydrocarbon reformer (*17*) must operate at a higher temperature than our SOFC. (iv) The single-chamber cell design provides a more compact cell stack. These advantages, as well as the above results, greatly enhance the position of SOFCs as the preferred electric power generation technique for vehicles in the foreseeable future.

References

1. E. P. Murray, T. Tsai, S. A. Barnett, *Nature* **400**, 649 (1999).
2. S. Park, J. M. Vohs, R. J. Gorte, *Nature* **404**, 265 (2000).
3. W. van Gool, *Philips Res. Rep.* **20**, 81 (1965).
4. G. A. Lousi, J. M. Lee, D. L. Maricle, J. C. Trocciola, U.S. Patent 4,248,941 (1981).
5. C. K. Dyer, *Nature* **343**, 547 (1990).
6. T. Hibino and H. Iwahara, *Chem. Lett.*, 1131 (1993).
7. C. A. Cavalca, G. Larsen, C. G. Vayenas, G. L. Haller, *J. Phys. Chem.* **97**, 6115 (1993).
8. I. Riess, P. J. van der Put, J. Schoonman, *Solid State Ionics* **82**, 1 (1995).
9. T. Hibino, S. Wang, S. Kakimoto, M. Sano, *Electrochem. Solid-State Lett.* **2**, 317 (1999).
10. B. C. H. Steele, *J. Power Source* **49**, 1 (1994).
11. C. Milliken, S. Guruswamy, A. Khandkar, *J. Electrochem. Soc.* **146**, 872 (1999).
12. H. L. Tuller and A. W. Nowick, *J. Electrochem. Soc.* **122**, 255 (1975).
13. A. T. Ashcroft *et al.*, *Nature* **344**, 319 (1990).
14. H. Uchida, M. Yoshida, M. Watanabe, *J. Phys. Chem.* **99**, 3282 (1995).
15. S. Mukerjee *et al.*, *Electrochem. Solid-State Lett.* **2**, 12 (1999).
16. M. Ciureanu and H. Wang, *J. Electrochem. Soc.* **146**, 4031 (1999).
17. N. Hashimoto, *Chem. Chem. Ind.* **50**, 1324 (1997).

28 February 2000; accepted 1 May 2000

Discovery of a Basaltic Asteroid in the Outer Main Belt

D. Lazzaro,[1]* T. Michtchenko,[2] J. M. Carvano,[1] R. P. Binzel,[3] S. J. Bus,[3] T. H. Burbine,[3] T. Mothé-Diniz,[1] M. Florczak,[4] C. A. Angeli,[1] Alan W. Harris[5]

Visible and near-infrared spectroscopic observations of the asteroid 1459 Magnya indicate that it has a basaltic surface. Magnya is at 3.15 astronomical units (AU) from the sun and has no known dynamical link to any family, to any nearby large asteroid, or to asteroid 4 Vesta at 2.36 AU, which is the only other known large basaltic asteroid. We show that the region of the belt around Magnya is densely filled by mean-motion resonances, generating slow orbital diffusion processes and providing a potential mechanism for removing other basaltic fragments that may have been created on the same parent body as Magnya. Magnya may represent a rare surviving fragment from a larger, differentiated planetesimal that was disrupted long ago.

The diversity of compositions of iron meteorites and nonchondritic stony meteorites (*1*) suggests an early period of heating, melting, and differentiation of planetesimals that were later disrupted and became asteroids in the main belt rather than accreting to form planets. In the main belt today, only the large (525-km diameter) asteroid Vesta (*2–4*) and its associated family of impact excavated fragments (*5–9*) have been considered to be basaltic remnants (representing the crust of a differentiated planetesimal) from this early epoch of solar system history. We report observations of a 30-km outer main-belt asteroid, 1459 Magnya, that also shows the characteristic signature of a basaltic surface.

In September 1998, we performed spectroscopic observations of Magnya that indicated its possible basaltic composition (*10*) at the European Southern Observatory at La Silla (ESO-Chile) (*11*). Additional observations of this asteroid were obtained in November 1999 and January 2000 with the double spectrograph on the 5-m Hale telescope at Palomar Observatory and in December 1999 with NSFCAM on the 3-m NASA Infrared Telescope Facility (IRTF) at Mauna Kea, Hawaii (*12*).

The ESO, Palomar, and Mauna Kea spectra of Magnya compared with the spectra of Vesta (Fig. 1) show similar absorptions near 1 and 2 μm, indicating a basaltic composition for Magnya. The basaltic nature of these surfaces is further confirmed by their match to basaltic achondrite meteorites, such as meteorites from the howardite, eucrite, and diogenite (HED) classes. Although Vesta has been suggested as a source for HED meteorites (*7–9, 13*), the implied ejection velocity (*7, 8*) for a fragment the size of Magnya being ejected from Vesta (at semimajor axis, a, of 2.36 AU) to Magnya's present location (a = 3.14 AU, e = 0.24, and i = 17°, where e and i are the orbit eccentricity and inclination, respectively) is in excess of 5 km/s. We consider this high velocity to exceed any plausible limit for linking Magnya as a fragment directly ejected from Vesta. The orbits of Magnya and Vesta do overlap (the perihelion distance of Magnya is less than the aphelion distance of Vesta), leaving open some possibility that Magnya is an ejected and dynamically evolved fragment from Vesta. However, the lack of other evidence for such a dynamical evolution of the Vesta family (*5–8*) makes this link unlikely. Therefore, we consid-

[1]Observatório Nacional, Departamento de Astrofísica, Rua Gal. José Cristino 77, 20921-400 Rio de Janeiro, Brazil. [2]Instituto Astronômico e Geofísico, Universidade de São Paulo, Av. Miguel Stefano 4200, 04301-904 São Paulo, Brazil. [3]Department of Earth, Atmospheric, and Planetary Sciences, Massachusetts Institute of Technology, 77 Massachusetts Avenue, Cambridge, MA 02139–4301, USA. [4]Centro Federal de Educacão Tecnológica do Paraná, Departamento de Física, Av. Sete de Setembro 3165, 80230-901 Curitiba, Brazil. [5]Jet Propulsion Laboratory, MS 183-501, 4800 Oak Grove Drive, Pasadena, CA 91109, USA.

*To whom correspondence should be addressed.